The Structure of Yb^{3+} Aquo Ion and Chloro Complexes in Aqueous Solutions at Up to 500 °C and 270 MPa

Robert A. Mayanovic* and Sumedha Jayanetti†

Department of Physics, Astronomy and Materials Science, Southwest Missouri State University, Springfield, Missouri 65804

Alan J. Anderson

Department of Geology, St. Francis Xavier University, P.O. Box 5000, Antigonish, Nova Scotia B2G 2W5, Canada

William A. Bassett

Department of Geological Sciences, Cornell University, Ithaca, New York 14853

I-Ming Chou

MS 954, U.S. Geological Survey, Reston, Virginia 20192

Received: January 16, 2002; In Final Form: April 29, 2002

We report here on X-ray absorption fine structure (XAFS) measurements used to determine the structure of the Yb^{3+} ion in aqueous solutions over a range of temperatures from 25 to 500 °C and pressures up to 270 MPa. Fluorescence Yb L_3-edge spectra were collected separately from nitrate (0.006*m* Yb/0.16*m* HNO_3) and chloride (0.006 *m* $YbCl_3$/0.017 *m* HCl) aqueous solutions within a hydrothermal diamond anvil cell. The Yb−O distance of the Yb^{3+} aquo ion in the nitrate solution exhibits a uniform reduction at a rate of 0.02 Å/100 °C, whereas the number of oxygens decreases from 8.3 ± 0.6 to 4.8 ± 0.7, in going from 25 to 500 °C. No evidence for nitrate complexes was found from measurements made on this solution. The Yb^{3+} is found to persist as an aquo ion up to 150 °C in the chloride aqueous solution. In the 300−500 °C range, chloro complexes are found to occur in the solution, most likely of the type $Yb(H_2O)_{\delta-n}Cl_n^{+3-n}$ ($\delta \approx 7$). The Yb−Cl distance of the chloro ytterbium(III) complexes is found to decrease uniformly at a rate of about 0.02 Å/100 °C, whereas the number of chlorines increases from 0.5 ± 0.3 to 1.8 ± 0.2 in the 300−500 °C temperature range. Conversely, the Yb−O distance undergoes a lower uniform reduction at a rate of 0.007 Å/100 °C, whereas the number of oxygens decreases from 8.3 ± 0.5 to 5.1 ± 0.3 in going from 25 to 500 °C in the same solution.

Introduction

Our understanding of solvation of ions in water under near critical and supercritical conditions is limited. Progressive hydrogen bond breaking in the network structure of water leads to reduced screening of ions with increasing temperature in the electrolytic fluid. The reduced screening results in increased ion−ion interaction, thereby directly affecting the stability of ion complexes at elevated temperatures. Consequently, the solubility of many organics increases in supercritical water under low-density (~0.1 g/cm^3) conditions, leading to applications in separations technology of organic waste products.[1,2] In addition, variation of the local fluid structure, resulting in the reduction of the dielectric constant, is thought to directly impact the structure and speciation of ion complexes in aqueous solutions with temperature.[3] However, detailed knowledge of water solvation and local structure in the vicinity of ions under elevated pressure−temperature (P−T) conditions is severely lacking. This can be directly attributed to the scarcity of data on the structure of ion complexes in hydrothermal solutions. Such data are requisite for a greater understanding of solution chemistry and geochemistry[4,5] and have relevance for development of nuclear and chemical waste remediation using supercritical fluids.[1] High P−T structure data of ions in aqueous solutions are also important for development of ab initio theories and molecular dynamics simulations of electrolytic fluids, under a broad range of thermodynamic conditions.

The series of lanthanide (Ln) ions offer an ideal system for a study of structure and related properties in hydrothermal fluids. The 4f electrons of these elements are very effectively shielded by the outermost electronic shells, resulting in very weak interactions with ligands of lanthanide complexes. Consequently, the lanthanides are thought to behave much like the alkali metals in the formation of complexes. In addition, the Ln^{3+} ions exhibit very uniform structure properties across the series, such as the lanthanide contraction effect, in ambient aqueous solutions. Studies of Ln-bearing aqueous solutions under ambient conditions are well established. X-ray diffraction,[6,7] neutron diffraction,[8,9] photoacoustic spectroscopy,[10] and Raman spectroscopy[11]

* To whom correspondence should be addressed. Fax: (417)-836-6226. E-mail: ram051f@smsu.edu.

† On leave from Department of Physics, University of Colombo, Colombo 3, Sri Lanka.

10.1021/jp020140q CCC: $22.00
Published on Web 06/14/2002

have been used to provide information on speciation and structure of lanthanide ions in aqueous solutions. X-ray absorption fine structure (XAFS) has also been applied to provide local structure information of lanthanide ions in room-temperature aqueous solutions.[12−14] Yamaguchi et al.[12] found detailed evidence for the lanthanide contraction effect from their systematic X-ray absorption fine structure (XAFS) study of the hydration structure of nearly the complete range of lanthanide ions. From their XAFS study of La^{3+}, Ce^{3+}, Nd^{3+}, Eu^{3+}, Yb^{3+}, and Y^{3+} ions in high-concentration chloride aqueous solutions, Allen et al.[14] found greater Cl^- complexation for the lighter lanthanides with a gradual decrease in approaching the heavier ones. Yb^{3+} and Y^{3+} ions showed no association with Cl^- ligands from their study made under ambient conditions. Investigations of the local structure of Y^{3+} in 0.1 M YCl_3-bearing aqueous solutions (with up to 2.5 M Cl) from 25 to 340 °C have been made using XAFS by Ragnarsdottir et al.[15]

Theoretical calculations of Ln speciation in aqueous solutions under elevated P−T conditions are well established. An extensive study involving thermodynamic calculations of stability constants of the complete range of lanthanide ions interacting with Cl^-, OH^-, NO_3^-, and other ligands in dilute aqueous solutions has been carried out by Haas et al.[16] However, there are very few spectroscopic studies of the structure of lanthanide ions in aqueous solutions at elevated temperatures and pressures. Wood found from a thermodynamic analysis of lanthanide ions in aqueous solutions that complex stability increases at elevated P−T conditions.[17] This was confirmed for Nd^{3+} complex formation with acetate and Cl^- ligands, from potentiometric measurements on hydrothermal solutions up to 225 °C.[18] Similar confirmation was made from solubility measurements on aqueous Yb^{3+}−oxalate complexes up to 80 °C[19] and on aqueous Nd^{3+} [20] and other Ln^{3+} chloro complexes at up to 300 °C.[21]

As noted above, XAFS has proven to be a very useful tool for the study of the structure of fluids. The two primary limitations, which have impeded progress in X-ray absorption spectroscopy of hydrothermal fluids, are corrosivity and signal efficiency of high P−T cells. Signal efficiency, owing to the thickness and type of window material of the cell, has been a particularly important barrier to overcome because the study of the complete Ln series and other light elements is otherwise precluded. We have successfully solved the problem of signal efficiency through recent improvements of the hydrothermal diamond anvil cell by laser drilling grooves in the diamond windows.[22] Our recent studies show that this cell is suitable for fluorescence XAFS measurements of very dilute high P−T solutions below the X-ray photon energy of 5500 eV.[23] The cell was successfully used to make the first study of its kind from XAFS measurements of 0.007 *m* La in 2% HNO_3 solution at up to 300 °C and 170 MPa.[24] In continuation of our investigations of the Ln series, we have recently made XAFS measurements of Yb^{3+} complexes in dilute high P−T aqueous solutions. Here we report on the first study of the structure of Yb^{3+} ion complexes from measurements of nitrate (0.006 *m* Yb/0.16 *m* HNO_3) and chloride (0.006 *m* $YbCl_3$/0.017 *m* HCl) aqueous solutions at conditions ranging from 25 °C and atmospheric pressure to 500 °C and 270 MPa.

Experimental Details

The Hydrothermal Diamond Anvil Cell. The hydrothermal diamond anvil cell, which was designed specifically for high P−T studies of hydrothermal solutions, has been described in detail elsewhere.[25] The cell consists of two opposed 1/8-carat diamonds mounted on tungsten carbide seats. The laser-milled

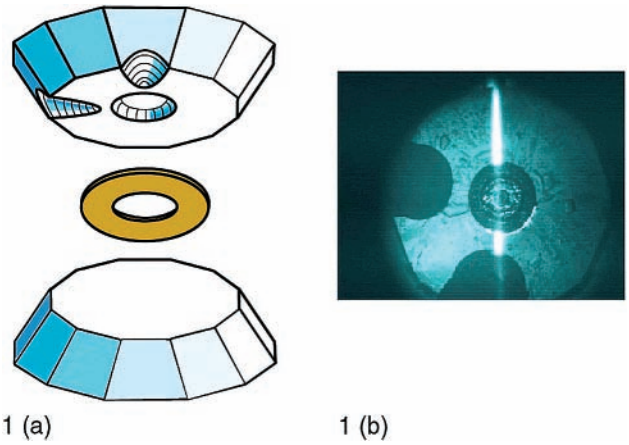

Figure 1. (a) Illustration showing how the diamond anvils of the hydrothermal cell are arranged, with a Re gasket sandwiched between, to seal a solution sample. The sample chamber is defined by the hole in the gasket and the central cavity in the grooved diamond anvil. The cell was used in inverted orientation during measurement with synchrotron X-ray beam, as depicted by the arrangement of the diamond anvils. (b) Visible fluorescence (vertical streak) showing the passage of incident X-rays through the sample chamber in the grooved diamond anvil of the hydrothermal diamond anvil cell. Note the two (circular) milled grooves in the anvil.

modifications to one of the anvils of the cell are illustrated in Figure 1a. One diamond has two laser-milled grooves, oriented at 90° to one another, which are 200−300 μm at the opening and extend to within 80 μm of a cavity, measuring 300 μm in diameter and 50−70 μm in depth, centered in the anvil face. In Figure 1b is shown the visible fluorescence from the passage of a focused X-ray beam through one of the laser-milled holes in the grooved anvil of the cell. For greatest ease of alignment during measurement with the synchrotron X-ray beam, the hydrothermal diamond anvil cell was inverted so that the grooved diamond was on the top. The seats containing the diamond anvils are mounted on upper and lower platens, which are drawn together by three screws and guided by three rods. The sample was heated externally by means of resistance heaters wound around the tungsten carbide seats that support the diamond anvils. Individual chromel−alumel thermocouples are attached to the upper and lower diamond anvil, separately, to measure the temperature of the sample. The temperature gradients, both in the vertical and horizontal orientation, are small owing to small sample size and high thermal conductivity of diamond. The corrections are typically less than 5 °C.

A fluid sample (solution plus vapor bubble) is placed within the confines of a 300 μm diameter hole of a 50−100 μm thick rhenium gasket and the cavity in the center of the anvil face of the grooved diamond. The anvil faces, about 1 mm across, seal the top and bottom of the sample hole + cavity as the anvils are driven together. Sample pressure in the hydrothermal diamond anvil cell is determined from equation of state of the sample fluid.[22,23]

Sample Preparation. A 0.006 *m* (1000 ppm) Yb in 0.16 *m* (1%) HNO_3 standard solution and 99.9% purity $YbCl_3 \cdot 6H_2O$ powder were obtained from the Aldrich Chemical Co. A solution having 0.006 *m* $YbCl_3$ and 0.017 *m* HCl (Cl:Yb ratio of 6:1) was prepared using distilled deionized water and a 6.0 N HCl solution. The solution was clear with no evidence of a precipitate during preparation. The pH values of the nitrate and of the chloride solutions were determined prior to loading into the cell to be 1.23 and 1.67, respectively. A micropipet was used to carefully load the solution samples into the chamber of the hydrothermal diamond anvil cell under a binocular microscope.

This method prevents overflow of the sample solution into the diamond grooves. Additional room-temperature XAFS spectra were measured from samples loaded separately into (300 μm o.d. and 280 μm i.d.) pure silica capillary tubes.

XAFS Data Acquisition. XAFS spectra were collected at the Yb L_3-edge (8944 eV) on the undulator PNC−CAT ID20 beam line of the Advanced Photon Source (APS), at the Argonne National Laboratory. XAFS data acquisition was accomplished by collection of the X-ray fluorescence signal using a 13-element Ge detector. The detector was placed in the standard horizontal 90° orientation to the incident X-ray beam. The synchrotron was operated at 7.0 GeV and 100 mA maximum fill current. A standard copper foil was used to calibrate the monochromator. The Si(111) crystals of the monochromator were detuned by 30−40% as a means of harmonic reduction in the incident X-ray beam. Each spectrum was measured for approximately 20 min. The slits before the monochromator were positioned at 2.4 mm (width) × 1.2 mm (height), whereas the ones after the monochromator were adjusted to 0.96 mm (width) × 0.875 mm (height). Kirkpatrick-Baez mirrors were used to focus the beam giving roughly a 25 μm circular spot with a flux of 5×10^{11} photons/second at the X-ray energy of 8900 eV. The incident and transmitted X-ray beam were detected using gas ionization chambers (10.2 and 30.5 cm lengths, respectively) filled with dry nitrogen gas. Up to six scans were collected at each P−T point. Small Bragg diffraction peaks in the spectra were observed occasionally. In this case, the cell was rotated by up to ±4 degrees relative to the incident beam direction, in the plane of the synchrotron radiation. This resulted in movement of the Bragg peaks in energy space by a sufficient amount so that the same region devoid of peaks from another scan could be used to replace a region containing a peak in one scan.

For both the nitrate and the chloride aqueous solution samples, small amounts of precipitate were formed and collected on the face of the bottom anvil inside the cell during the experiment under elevated P−T conditions (150 °C and equilibrium vapor pressure and above). In both cases, the color of the precipitate appeared to be brown or black. The precipitates were sufficiently out of the incident X-ray beam (~100 μm below) in the sample so that only the solution was measured. XAFS spectra measured from the precipitate formed within the nitrate solution show that it is most likely a highly disordered or an amorphous Yb_2O_3 phase. Additional analyses on the precipitates were not possible because of their small quantities.

To test the effect of incident X-ray beam flux intensity on the formation of the precipitates, the experiment was repeated on a newly loaded ytterbium(III) chloride sample under reduced flux conditions (~8×10^{10} photons/second at 8900 eV). Beam reduction was accomplished using a 200 μm Al (99.99% purity) foil placed in the incident X-ray beam immediately after the Kirkpatrick-Baez focusing mirrors and in front of the I_0 detector. In this case, additional fine slits were placed in front of the sample, to eliminate scattered radiation. The precipitate was nearly or completely eliminated during the repeated experiment. In this way, the initial stoichiometry of the ytterbium(III) chloride solution sample was preserved throughout the repeated experiment. We speculate that the precipitate formation may have been triggered by beam-induced radiolysis effects occurring in aqueous solutions exposed to high-brilliance X-ray radiation.[26] The results discussed below are from analysis of XAFS spectra of the ytterbium(III) chloride solution measured under reduced incident X-ray beam flux conditions. Because we only find evidence for Yb^{3+} aquo ion speciation from measurements of the ytterbium(III) nitrate solution sample under normal X-ray beam flux conditions, we found it unnecessary to repeat the experiment under reduced flux conditions. In addition, the onset of the Yb L_3 X-ray absorption edge was virtually identical (~8646 eV) for the solution samples measured at room temperature in capillary tubes, under elevated P−T conditions in the HDAC, and for the Yb precipitate. This provides evidence that the ytterbium ion remained in the trivalent state in the nitrate and chloride solutions under elevated P−T conditions.

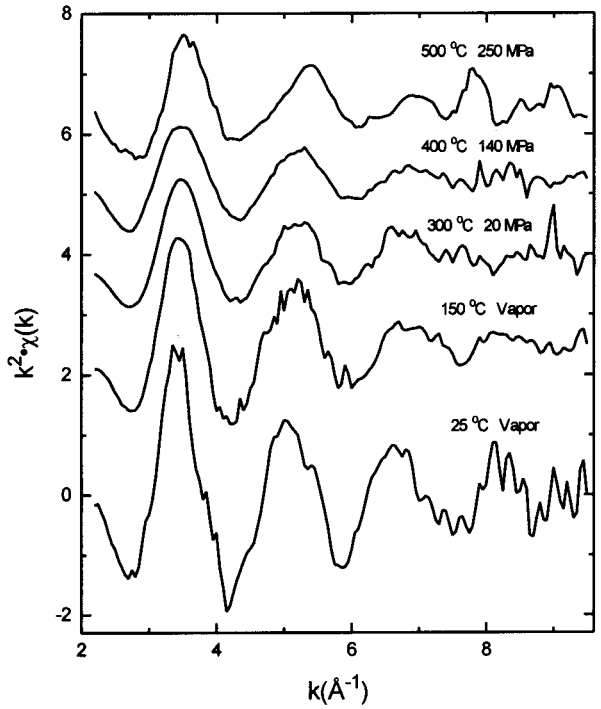

Figure 2. Isolated k^2 weighted $\chi(k)$ data, reduced from XAFS spectra of ytterbium(III) nitrate solution at P−T conditions ranging from ambient to 500 °C and 250 MPa.

Data Analysis. The fluorescence XAFS are calculated by normalizing the measured fluorescence signal I_f with respect to the incident X-ray beam intensity I_0. Up to six scans collected at the same P−T point were chosen for averaging of the XAFS spectra measured from each of the solutions. The threshold edge energy E_0 was determined by finding the point of inflection from the derivative of each of the averaged spectra. Its value was found to be ~8940.5 and ~8946.4 eV, respectively, for the spectra of nitrate and chloride solutions. A difference of ~6.0 eV of the edge position occurred because of a crude step size chosen in the Yb L_3-edge region during measurement of the ytterbium(III) nitrate solution sample. To reduce some of the noise occurring in the spectra measured from the nitrate solution, two-point adjacent averaging was used in the energy range $E >$ ~9010 eV ($k >$ ~4.3 Å^{-1}). Similarly, for XAFS spectra measured from the ytterbium(III) chloride solution sample, one-point adjacent averaging was applied in the energy range $E >$ ~9130 eV ($k >$ ~6.9 Å^{-1}). XAFS oscillations, $\chi(k)$, were isolated using an automated background subtraction program (AUTOBK) developed by Newville et al.[27] During this procedure, k^2 weighting was used on raw absorption data in the k range from 0.6 to 11 Å^{-1}. Using 6−7 knots in the spline resulted in obtaining the most suitable background function for $\mu_0(E)$, the monotonically varying part in the raw absorption spectra above the edge, in isolating $\chi(k)$ data. Figures 2 and 3 show the k^2 weighted $\chi(k)$ data at each P−T point, reduced from the XAFS spectra of the nitrate and chloride aqueous solutions, respectively.

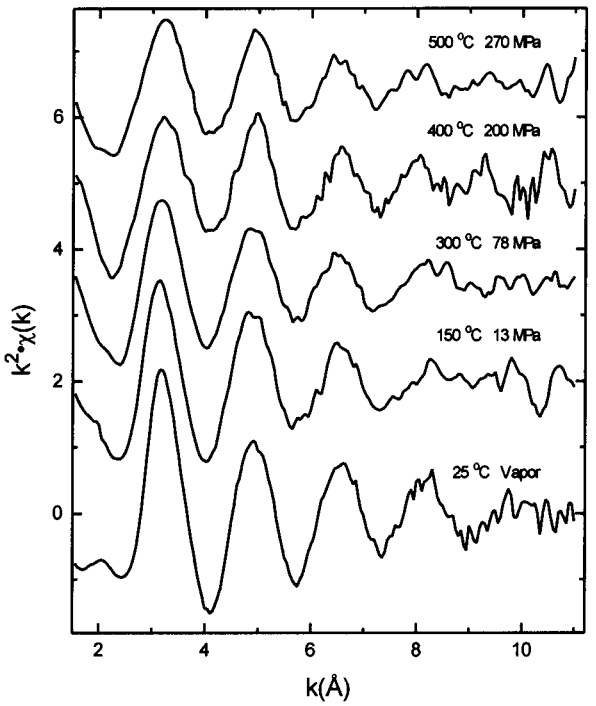

Figure 3. Isolated $k^2\chi(k)$ data, generated from XAFS spectra of ytterbium(III) chloride solution for P−T values ranging from ambient to 500 °C and 270 MPa.

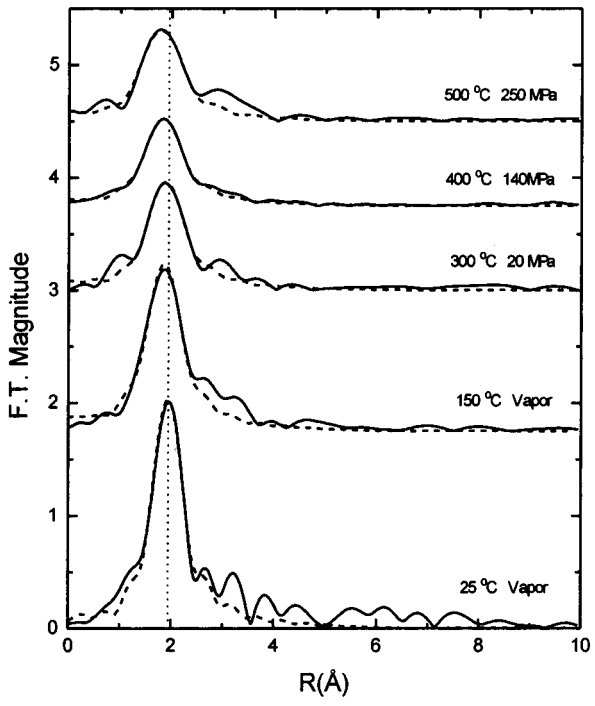

Figure 4. Magnitude of Fourier transforms of the $k^2\chi(k)$ data shown in Figure 2 (solid lines) calculated in the k range of 2.3−9.0 Å^{-1} and the corresponding best fits (dashed lines) as a function of temperature and pressure up to 500 °C and 250 MPa. Note: The gradual shift of the primary peak centered near 2 Å in the Fourier transform data toward lower R values is indicative of the Yb−O bond contraction with temperature.

The data analysis was made using the FEFFIT2.54 software program.[28,29] This program employs a nonlinear, least-squares fit to the theoretical standards calculated using FEFF8 theoretical code.[30] Fitting was made simultaneously in r space (the Fourier transformed space) and filtered k space (inverse Fourier transformed space). Fitting parameters included the coordination number (N_i), the radial distance (R_i), the XAFS Debye−Waller factor (σ_i^2), and ΔE_0, which compensates for the mismatch between E_0 and its theoretical estimate.

Figures 2 and 3 show presence of significant noise in the $\chi(k)$ spectra beyond about 10.0 Å^{-1} in k space. In addition, because the backscattering amplitude for oxygen is significantly attenuated beyond about 6 Å^{-1}, k^2 weighting was selected for analysis of spectra measured from the ytterbium(III) nitrate solution.[31] This selection compensates for signal attenuation with k while limiting possible introduction of errors due to noise in the high k region in the analysis of $\chi(k)$ data. A fitting model containing eight equidistant oxygens surrounding a central ytterbium atom in a cubic arrangement (Yb−O_8) was used for spectral analysis. Only single scattering Yb−O paths were employed in formulating the model χ(k) data using FEFF8. Fitting in r space was accomplished on data (shown in Figure 4) that were obtained by Fourier transforming the $\chi(k)$ data in the k range of 2.3−9.0 Å^{-1}. For fitting in k space, the filtered $\tilde{\chi}(k)$ data shown in Figure 5 were obtained by inverse transforming the Fourier transform data in the 1.0−3.0 Å range. The k range was limited to 7.5 Å^{-1} during analysis of data measured at 500 °C, to avoid an artifact attributed to noise occurring near 8 Å^{-1} in χ(k) data. All fitting parameters including ΔE_0 were allowed to vary during fitting. In comparison to its value under ambient conditions (12.5 eV), ΔE_0 was found to be approximately ∼11 eV for spectra measured under elevated P−T conditions, leading to a consistent discrepancy of ∼2.0 eV. We speculate that the larger value of ΔE_0 is indicative of significant surface adsorption on and/or diffusion of Yb^{3+} into the walls of the capillary holding the solution sample during room-temperature measurements.[32]

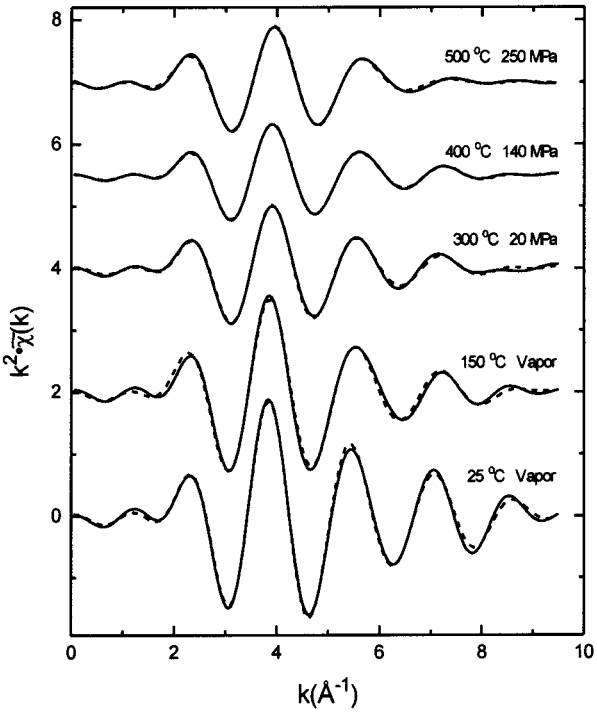

Figure 5. Filtered $k^2\tilde{\chi}(k)$ data (solid lines) obtained by inverse transforming the Fourier transform data shown in Figure 4 in the range 1.0−3.0 Å and the corresponding best-fits (dashed lines), as a function of temperature and pressure up to 500 °C and 250 MPa.

For similar reasons as discussed above, k^2 weighting was selected for analysis of spectra measured from the ytterbium-(III) chloride solution. The fitting procedure involved processing Fourier transform data shown in Figure 6, which were obtained by transforming the $\chi(k)$ data in the 2.5−10.0 Å^{-1} range.

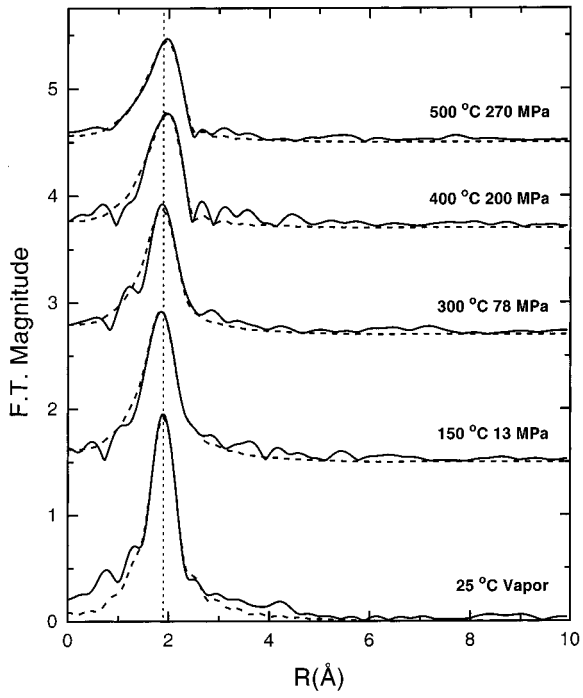

Figure 6. Magnitude of Fourier transforms of the $k^2\chi(k)$ data shown in Figure 3 (solid lines) calculated in the k range of 2.5−10.0 $Å^{-1}$ for P−T values up to 500 °C and 270 MPa. The best-fit curves (dashed lines) of the Fourier transform data are also shown. Note: As in Figure 3, the primary peak shifts are consistent with Yb−O bond contraction effects up to 150 °C. However, beyond 300 °C, a reversal of the trend is observed as Yb^{3+}−Cl^- association becomes significant with increasing temperature.

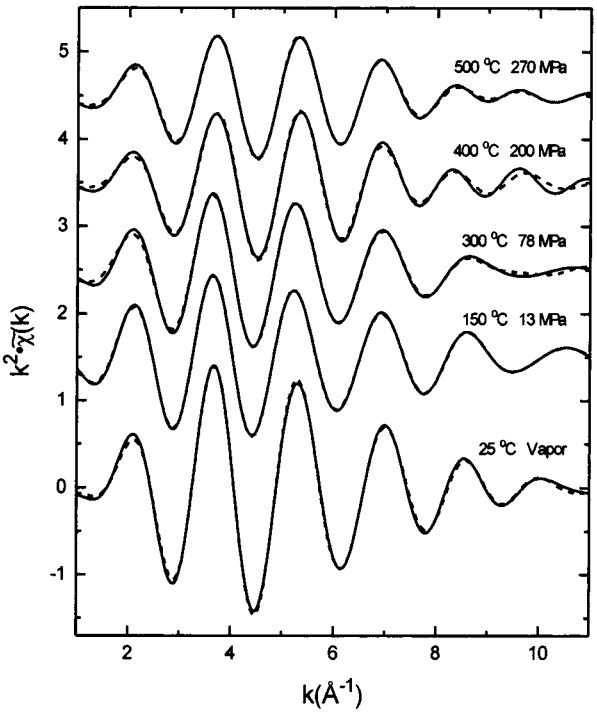

Figure 7. Filtered $k^2\tilde{\chi}(k)$ data (solid lines) generated by inverse Fourier transforming the data shown in Figure 6 in the range 1.4−2.8 Å and the corresponding best-fit curves (dashed lines) as a function of temperature and pressure up to 500 °C and 270 MPa. Interference effects occurring due to mixed coordination of the Yb^{3+} cation with oxygens and chlorines are evident at ∼8 $Å^{-1}$ and above for data measured at 300 °C and beyond.

Similarly, the $\tilde{\chi}(k)$ data shown in Figure 7 were obtained by inverse transforming of the Fourier transform data in the 1.4−2.8 Å range. The Yb−O_8 single shell model described above was used to fit spectra measured at 25 and 150 °C. For spectra measured at 300 °C and above, a new model was used as necessitated by the evolving structure in the data. This model has four equidistant oxygen atoms in the first shell and a similar arrangement of chlorine atoms in the second shell. Only single scattering paths were used for both oxygen and chlorine backscatterers. Two different ΔE_0 values, which were kept fixed during fitting, were used for Yb−O (4.0 eV) and Yb−Cl (6.5 eV) paths, respectively. Variation of other fitting parameters gave good results with somewhat higher uncertainties attributable primarily to noise in the spectra. By constraining the Debye−Waller factors, these uncertainties were minimized. This was necessitated in part by the interference between the contributions to each spectrum from oxygen and chlorine backscatterers, respectively. Adding to this is the finite range of the $\chi(k)$ data and relatively close Yb−Cl and Yb−O distances. Application of the double shell model to fitting spectra measured at room temperature did not yield any physically meaningful results, thus justifying the use of the Yb−O_8 single shell model. We have followed the example of Allen et al.[14] and used an amplitude reduction factor $S_0^2 = 1.0$ in the course of fitting. The fitting results are tabulated in Table 1 with the goodness of the fit given by the $\mathscr{R}$ factor, which, in general, is <0.05 for a good fit. Finally, anharmonic effects were considered during analysis of the data, by inclusion of the C_3 and C_4 anharmonic parameters in the cumulant expansion, but were found to be negligible.

TABLE 1: Structure Results from Fitting of XAFS Spectra Measured from a 0.006 *m* Yb/0.16 *m* HNO_3 Aqueous Solution

temp	$\Delta E_{0(Yb-O)}$	N_O	R_{Yb-O}	σ^2_{Yb-O}	$\mathscr{R}$ factor
25 °C	12.5 ± 0.5	8.3 ± 0.6	2.33 ± .01	0.007 ± .001	0.006
150 °C	10.8 ± 0.9	7.8 ± 0.8	2.29 ± .01	0.013 ± .003	0.016
300 °C	11.3 ± 1.0	6.2 ± 0.7	2.28 ± .01	0.01 6± .003	0.006
400 °C	10.4 ± 1.1	4.8 ± 0.6	2.26 ± .01	0.017 ± .003	0.008
500 °C	10.9 ± 1.1	4.8 ± 0.7	2.24 ± .02	0.017 ± .004	0.011

Discussion

Nitrate Solution. Our room temperature results shown in Table 1 are generally in excellent agreement with the structure results for hydrated Yb^{3+} obtained from studies by Kurisaki et al.,[7] Helm et al.,[8] Cossy et al.,[9] Yaita et al.,[13] and Allen et al.[14] Although Habenschuss and Spedding[6] and Yamaguchi et al.[12] have not measured the structure of the hydrated Yb^{3+} ion, they have done so for most of the lanthanides including Tm and Lu. These results, when interpolated for the hydrated Yb^{3+} ion, show excellent agreement with our results. Although our measurements are insensitive to the precise geometry of the inner hydration shell, the number of oxygen ligands (8.3) is consistent with the square antiprismatic structure of the Yb^{3+} aquo ion determined from molecular dynamics simulations made by Kowall et al.[33]

Yaita et al.[13] found evidence for bidentate coordination of the lanthanides ranging from Nd to Lu, including for the Yb^{3+} ion, to the oxygens of the nitrate ion only for solutions having the highest HNO_3 concentrations. The Ln−O_2NO distances of the nitrate complexes were reported to be about 0.1 Å longer than the Ln−OH_2 distances. The presence of the nitrogen backscatterer was revealed by the appearance of a peak in the Fourier transform data near 3.8 Å and by beating or interference

TABLE 2: Structure Results from Fitting of XAFS Spectra Measured from a 0.006 *m* $YbCl_3$/0.017 *m* HCl Aqueous Solution

temp	$\Delta E_{0(Yb-O)}$	$\Delta E_{0(Yb-Cl)}$	N_O	N_{Cl}	R_{Yb-O}	R_{Yb-Cl}	σ^2_{Yb-O}	σ^2_{Yb-Cl}	$\mathcal{R}$ factor
25 °C	7.2 ± 0.5		8.3 ± 0.5		2.328 ± .007		0.007 ± .001		0.003
150 °C	4.7 ± 0.4		8.5 ± 0.4		2.316 ± .006		0.012 ± .001		0.002
300 °C	4.0	6.5	6.5 ± 0.5	0.5 ± 0.3	2.306 ± .007	2.60 ± .04	0.012	0.006	0.009
400 °C	4.0	6.5	5.1 ± 0.6	1.6 ± 0.3	2.29 ± .01	2.57 ± .01	0.016	0.007	0.014
500 °C	4.0	6.5	5.1 ± 0.3	1.8 ± 0.2	2.294 ± .008	2.566 ± .009	0.019	0.009	0.004

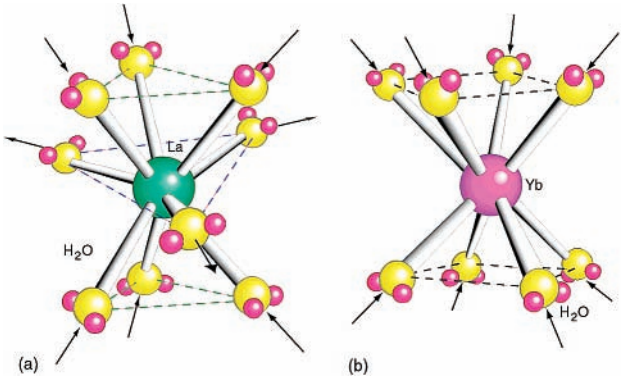

Figure 8. (a) Schematic diagram showing how the three equatorial waters shift outward, whereas the six water molecules residing in the tricapped trigonal prismatic sites shift inward as the structure of the hydrated La^{3+} aquo ion undergoes relaxation at elevated temperatures. (b) A similar diagram showing how the eight water molecules residing in the square antiprismatic sites are contracted inward toward the Yb^{3+} aquo ion in aqueous solutions under elevated temperatures. The antiprismatic structure was determined from molecular dynamic simulations by Kowall et al.[33]

features in the $\chi(k)$ data (indicative of multiple shell structure surrounding the absorber). Because these indicators were not present in our structure results or in the data, we conclude that the Yb^{3+} ion does not exhibit nitrate complex formation under all P−T conditions of our study.

Furthermore, as shown in Table 1 and also in the data shown in Figures 2, 4, and 5, Yb^{3+} persists as an aquo ion in the aqueous solution throughout the complete P−T range of our study. The Yb−O interatomic distance exhibits a uniform reduction at a rate of 0.02 Å/100 °C, in going from 25 to 500 °C. Several groups have observed local structure relaxation of hydrated ions with temperature in hydrothermal solutions. Bond-length reduction of the Rb^+ aquo ion was reported by Fulton et al.[34] and of the Ag^+ [35] and Sr^{2+} [36] aquo ions by Seward et al., from XAFS measurements made under elevated P−T conditions. In their study on yttrium chloride solutions up to 340 °C, Ragnarsdottir et al.[15] find that the Y−O interatomic distance remains constant with temperature.

The bond contraction is accompanied by a uniform reduction in the number of water molecules in the first hydration shell of the Yb^{3+} aquo ion with increasing temperature. As shown in Table 1, the average number of oxygens is found to decrease from 8.3 ± 0.6 at 25 °C to 4.8 ± 0.7 at 500 °C, indicating a 42% reduction over this temperature range. Similar reductions in hydration waters surrounding various metal cations have been reported from other XAFS studies made on aqueous solutions at elevated P−T conditions.[34−39] In addition, Ragnarsdottir et al.[15] find the Y^{3+} aquo ion to undergo a reduction from 9 to 10 water molecules at 25 °C to about 8 at 340 °C.

The relaxation behavior of the hydrated Yb^{3+} ion with temperature is considerably different from that of the La^{3+} aquo ion examined in our previous study.[24] The contrast in relaxation of the structure of these two hydrated ions is illustrated using Figure 8 parts a and b. Three oxygens (most likely in the equatorial plane) of the La^{3+} ion hydration shell are shifted outward by 0.20 ± 0.04 Å, in going from 25 to 300 °C. Conversely, six oxygens (in the tricapped trigonal prismatic sites) are contracted inward by 0.11 ± 0.03 Å in the same temperature range. There was no reduction of hydration waters of the La^{3+} aquo ion up to 300 °C observed in our previous study. The true nature of the mechanism responsible for the relaxation of the hydrated La^{3+} ion has yet to be determined. It may be very likely that several competing mechanisms are responsible for the exact type of relaxation of the lighter lanthanide aquo ions, such as size effects, field strength, the nature and strength of the ligand−cation interaction, and potentially others. We comment further on the nature of Yb^{3+} aquo ion relaxation in the section below.

Chloride Solution. Our results from analysis of spectra measured from the chloride solution sample (in Table 2) at room temperature indicate that the Yb^{3+} ion is hydrated with approximately eight equidistantly positioned water molecules in the inner hydration sphere. We do not find evidence for chloro complex formation in this solution at room temperature. These results are in excellent agreement with those obtained by Cossy et al.,[9] Yaita et al.,[13] and Allen et al.[14] In addition, these results are consistent with our structure data for the hydrated Yb^{3+} ion in our nitrate solution measured at room temperature.

Complete hydration of the Yb^{3+} ion was found to persist up to 150 °C. At 300 °C and beyond, the solution exhibits formation of most likely stepwise $Yb(H_2O)_{\delta-n}Cl_n^{+3-n}$ complexes, where $\delta \approx 7$ and n is an integer ranging from 0 to 3. The combination of innershell hydration and chloro complex formation of the Yb^{3+} ion is most evident at first glance in the interference features occurring in the higher k range (~8 $Å^{-1}$ and above) of the $\chi(k)$ data shown in Figure 3 and of the filtered $\tilde{\chi}(k)$ data shown in Figure 7, for spectra measured at 300 °C and beyond. This was confirmed in failed attempts to fit these data using a single-shell hydration model. Forcing such fits did not yield physically meaningful results. The data show a steady increase of the interference features with temperature, in going from 300 to 500 °C. This is reflected in a broadening of the primary peak shape, centered near 2 Å, in the Fourier transform data over the same temperature range.[40] This suggests a steady increase in the average number of chlorines in proportion to water molecule ligands of the Yb^{3+} ion in the aqueous solution with temperature. Our results from fitting confirm this general trend. As shown in Table 2, the average number of oxygens (of the water molecules) coordinated to the Yb^{3+} ion decreases uniformly from 6.5 ± 0.5 at 300 °C to 5.1 ± 0.3 at 500 °C, whereas the average number of chlorines increases uniformly from 0.5 ± 0.3 to 1.8 ± 0.2 over the same temperature range. Figure 9 shows a depiction of the $Yb(H_2O)_5Cl_2^+$ complex, which is predominant at 500 °C in the chloride solution. As mentioned above, our measurements provide insufficient information to detail the symmetry of the complex. Equilibrium thermodynamic calculations of stability constants of chloro ytterbium(III) complexes in dilute aqueous solutions carried out by Haas et al.[16] are in general agreement with our results. Furthermore, the considerably lower stability constants of nitrate ion complexes in comparison to that of chloro complexes of Yb^{3+}

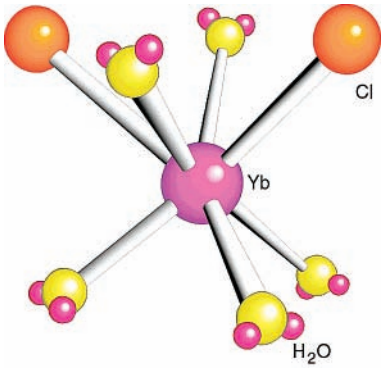

Figure 9. Depiction of the $Yb(H_2O)_5Cl_2^+$ complex, which is predominant at 500 °C in the chloride solution. This is one of the stepwise $Yb(H_2O)_{\delta-n}Cl_n^{+3-n}$ complexes ($\delta \approx 7$, $n = 0$, 1, 2, and 3) which are found to be stable in the solution from 300 to 500 °C. Note that our results give insufficient information on the precise symmetry of the complex.

predicted by these authors are consistent with the temperature-dependent structure results presented here.

The only directly relevant study that can be used for comparison to our study is by Ragnarsdottir et al.[15] of yttrium chloride aqueous solutions at up to 340 °C. No evidence for chloro complexes of yttrium(III) ions even for the highest Cl:Y ratio (28:1) solution at any temperature was reported from their study. It is not obvious to us why yttrium(III) chloride aqueous solutions would exhibit such different speciation behavior. Because the 4p electrons of the Y^{3+} ion play a very similar role to the 4f electrons of the Ln^{3+} ions, it would seem that chloro speciation of the former under the given conditions should be in the least comparable to that of the Yb^{3+} ion. It is possible that the experimental conditions (e.g., pH of solutions under elevated P−T conditions) may have been sufficiently different to account for the different speciation behavior in the yttrium-(III) chloride and ytterbium(III) chloride solutions. More study is needed to resolve these differences.

Note the consistently lower Debye−Waller factor values corresponding to Yb−Cl in comparison to those of Yb−O coordination. Because the Yb−O Debye−Waller factors are quite consistent as a function of temperature between the chloride and nitrate solutions and provided that the stepwise complexes occurring in the former are of the type $Yb(H_2O)_{\delta-n}Cl_n^{+3-n}$, then we have to exclude significant static disorder in the structure of these complexes. Thus, the difference between the Yb−O and Yb−Cl Debye−Waller factors can be attributed primarily to the difference in mass and vibrational characteristics of the two ligands (H_2O and Cl^-) in the coordination with the Yb^{3+} ion. The latter is a direct reflection of the nature of interaction between the ligand type and the Yb^{3+} ion.

Just as with the Yb−O distance of the Yb^{3+} aquo ion in the nitrate solution, the average Yb−Cl distance of the chloro ytterbium(III) complexes in the chloride solution undergoes a uniform reduction at a rate of about 0.02 Å/100 °C, in going from 300 to 500 °C. Several groups have reported bond length contraction occurring in metal halide complexes with temperature in hydrothermal solutions. A common metal−chlorine bond length reduction, occurring at a rate of about 0.01 Å/100 °C with temperature, was reported for chloro zinc(II) complexes in aqueous fluids by Anderson et al.[41] and by Mayanovic et al.[42,43] We have also reported similar results for bromo zinc(II) complexes[3,44] and for chloro iron(II) complexes.[45] Interestingly, Hoffman et al. obtained results showing expansion of the nickel−oxygen distance and a contraction of the nickel−bromine distance with temperature, from XAFS measurements made on nickel bromide aqueous solutions.[39] We find a uniform but lower rate of Yb−O distance reduction of about 0.007 Å/100 °C, in going from 25 to 500 °C, in the ytterbium(III) chloride solution compared to in the ytterbium(III) nitrate solution. The discrepancy in the rate of Yb−O distance contraction with temperature may be a result of speciation differences in the two solutions. In the nitrate solution, the Yb^{3+} persists as an aquo ion, whereas the chloride solution exhibits most likely stepwise $Yb(H_2O)_{\delta-n}Cl_n^{+3-n}$ complexes. The mixed inner shell environment made up of waters and chlorines may require slightly longer Yb−O distances upon contraction of the Yb−Cl bonds in order to maintain electrostatic equilibrium. In addition, it is possible that interference effects because of the nearly equidistant oxygen and chlorine backscatterers may have in part contributed to the discrepancy during the analysis of spectra measured from the chloride solution. We note that anharmonic effects were considered in the analysis of our data. Because the structure of simple metallic complexes is essentially molecular in nature, free volume effects such as one might encounter in liquids and certain glasses can be ignored.[46]

From our investigations of anion−oxygen bond breaking in zinc bromide solutions, a greater than 60% reduction in bromine−oxygen bonds was found for both the $ZnBr_4^{2-}$ complex and the Br^- aquo ion in going from 25 °C to 500 °C.[3] It was determined that the bromine ions and the oxygens of the waters are weakly hydrogen bonded. Generalizing these results to the present study, we attribute the relaxation of the structure of chloro ytterbium(III) complexes and Yb^{3+} aquo ions directly to hydrogen bond breaking and commensurate reduction of the outerhydration shell waters in approaching supercritical conditions in the aqueous solutions. The relaxation mechanism is conjectured to occur because of unbalanced ytterbium(III)−ligand interaction forces contracting the ligands inward toward the cation as the weak ligand-HOH bonds are broken at elevated temperatures. Such effects are quite interesting because they offer clues to the nature of cation−ligand interaction and to the physical properties of water solvation with temperature. It is very likely that ab initio molecular dynamics calculations made by Weare and co-workers will in the future give considerably more insight into the chemi-physical properties of such fluids.[47,48] As we have reported in the past, we find that, for the range accessible for our studies (up to 1 GPa), pressure plays a negligible role in comparison to temperature in the relaxation effects of the structure of complex ions.[3,24,42,44]

Note that the rate of reduction of innershell hydration waters with temperature of Yb^{3+}, as shown by N_O values in Tables 1 and 2, is nearly identical in both the nitrate and chloride solutions. Furthermore, the total number of Yb^{3+} ligands remains below eight ($N_O + N_{Cl} \approx 7$) in the 300−500 °C range. Thus, it appears that the Cl^- ligands undergo complex formation with Yb^{3+} upon the shedding of some of the innershell hydration waters. We infer from these results that the chloro ytterbium-(III) complexes found in the ytterbium chloride solution under elevated P−T conditions, exist reciprocally as stepwise $Yb(H_2O)_{\delta-n}Cl_n^{+3-n}$ complexes.

Comparison to Theoretical Calculations and Applications in Geochemistry. Comparison of Yb^{3+} and La^{3+} (from previous study) aquo ion behavior under elevated P−T conditions offers a glimpse into characteristics of lanthanide ions in hydrothermal environments. From their molecular dynamics simulation studies, Kowall et al.[33,49] find both the coordination number and the hydration enthalpy values for Nd^{3+}, Sm^{3+}, and Yb^{3+} aquo ions, to be in good agreement with experimental values. Conversely, whereas the kinetic exchange rates (in the first

hydration shell) were determined to be the largest for Sm^{3+}, the value for the Yb^{3+} aquo ion was predicted to be larger than for the Nd^{3+} aquo ion, in disagreement with experimental results. Because we find that the Yb^{3+} aquo ion sheds water ligands in going from 25 to 300 °C (from ~8 to ~6) and the La^{3+} aquo ion does not, we conclude that the former is less stable under increased temperature conditions than the latter. It is unclear how the measured or simulated kinetic exchange rate data are related to our results because of lack of comparable high-temperature values. We speculate that coordination symmetry of the waters in the innerhydration shell and/or the cation size (i.e., the lanthanide contraction effect) may play a significant role in the shedding of the waters under elevated P−T conditions. In essence, the combined contraction of the waters in the trigonal tricapped sites and expansion of the remaining ones in the equatorial sites and the larger ionic size of La^{3+} aquo ion may result in more stability than mere contraction of waters and the smaller ionic size of Yb aquo ion at high temperatures. It would be very useful to attempt molecular dynamics simulations, using an approach such as that of Kowall et al.,[33,49] on the same lanthanide aquo ions under elevated P−T conditions. Such calculations should address the question of whether a model-oriented, classical molecular dynamics approach is sufficient in treating the many body interactions in the hydration of the Ln^{3+} aquo ion.

Our results for chloro speciation of Yb^{3+} in the chloride solution under elevated P−T conditions qualitatively agree well with thermodynamic calculations made by Haas et al.[16] and are in agreement with results from solubility measurements made by Gammons et al.[21] These calculations do not explicitly account for partially hydrated stepwise $Yb(H_2O)_{\delta-n}Cl_n^{+3-n}$ complexes, as our results indicate to exist in such hydrothermal solutions. However, because these are based on experimentally derived association constants of Ln^{3+} with Cl^- under ambient conditions, the thermodynamic calculations most likely have a direct bearing on our results. Haas et al.[16] predict that La^{3+} chloro complexes are more stable under elevated P−T conditions than Yb^{3+} chloro complexes. This is in agreement with the results of Allen et al.[14] from XAFS measurements of chloride-rich aqueous solutions containing lanthanide ions at room temperature. They find weak chloride association with La^{3+} but none with Yb^{3+}. It appears then that kinetic exchange rate (assuming that variations across the lanthanide series are maintained at elevated temperatures) and shedding of waters may not be the only determinative factors in chloro Ln^{3+} complex formation under elevated P−T conditions. It is likely that size effects and other structure factors may play an important role in determining the stability of chloro and other Ln complexes in hydrothermal environments.

The extent of solubility and mobility of the lanthanides in natural fluids has been a source of considerable disagreement. A review of the literature pertaining to metamorphic processes has been made by Grauch.[50] Speciation and structural data of Ln^{3+} ions in hydrothermal solutions are much needed in order to provide more insight on the subject. Ours is a significant result because it provides direct evidence for significant Yb^{3+} solubility in acidic saline hydrothermal fluids. Although such fluids are not representative of most natural systems, our results should eventually help explain the transport of this element in the lithosphere in diagenetic, metamorphic, or hydrothermal alteration environments. In addition, comparison of innershell hydration behavior between the La^{3+} and Yb^{3+} aquo ions at elevated temperatures suggests that this may affect the sequence of deposition of various lanthanides in hydrothermal systems. Dramatic mineralogical evidence for such sequential deposition is provided in sequential banding in fluorite and other minerals.[51] Details on how such behavior is affected by Ln^{3+}-bearing saline-rich fluids will have to await our future studies involving investigations of other lanthanide(III) chloride solutions under elevated P−T conditions.

Conclusions

Yb L_3-edge XAFS spectra were measured separately from a nitrate (0.006 *m* Yb/0.16 *m* HNO_3) and chloride (0.006 *m* $YbCl_3$/0.017 *m* HCl) aqueous solutions, from 25 to 500 °C and up to 270 MPa. The Yb^{3+} is found to persist as an aquo ion in the nitrate solution throughout the P−T range of the study. The Yb−O distance exhibits a uniform reduction rate of 0.02 Å/100 °C, whereas the number of oxygens is found to decrease from 8.3 ± 0.6 to 4.8 ± 0.7, in going from 25 to 500 °C in the nitrate solution. In the chloride aqueous solution, Yb^{3+} persists as an aquo ion up to 150 °C. In the 300−500 °C range, chloro complex formation occurs in the solution, most likely in the form of $Yb(H_2O)_{\delta-n}Cl_n^{+3-n}$ complexes ($\delta \approx 7$). The average Yb−Cl distance of the chloro ytterbium(III) complexes reduces uniformly at a rate of about 0.02 Å/100 °C, in going from 300 to 500 °C. The number of Cl ligands surrounding Yb^{3+} increases from 0.5 ± 0.3 to 1.8 ± 0.2 over the same temperature range. The Yb−O average distance is reduced uniformly at a rate of 0.007 Å/100 °C, whereas the number of oxygens similarly reduces from 8.3 ± 0.5 to 5.1 ± 0.3 in going from 25 to 500 °C in the same solution. The relaxation in the structure of the Yb^{3+} aquo ion and of the chloro ytterbium(III) complexes is attributed to hydrogen bond breaking occurring in the outer hydration shell, resulting in the unbalanced Yb−ligand interaction forces contracting the ligands inward toward the cation at elevated temperatures.

Acknowledgment. We thank Steve Heald and others at PNC-CAT beam line, Robert Gordon of Simon Fraser University, and SMSU students Zachary Collard and Sonya McDaniel for assistance on our experiments at the Advanced Photon Source. This research was funded by a grant from the Research Corporation to R.A.M. We thank the Natural Sciences and Engineering Research Council of Canada (NSERC) for funding this research through a grant to A.J.A. and through a Major Facility Access Grant. The U.S. Department of Energy, Basic Energy Sciences, Office of Science, under Contract No. W-31-109-Eng-38 and DE-FG03-97ER45628 (PNC-CAT) supported the use of the Advanced Photon Source. This paper was improved by the useful comments of Robert Seals, Paul Barton, and an anonymous reviewer.

References and Notes

(1) Shaw, R. W.; Brill, T. B.; Clifford, A. A.; Eckert, C. A.; Franck, E. U. *Chem. Eng. News* **1991**, *69*, 26−39.

(2) Tester, J. W.; Holgate, H. R.; Armellini, F. J.; Webley, P. A.; Killilea, W. R.; Hong, G. T.; Barner, H. E. In *Emerging Technologies in Hazardous Waste Management III*; Tedder, D. W., Pohland F. G., Eds.; American Chemical Society: Washington DC, 1993; pp 34−76.

(3) Mayanovic, R. A.; Anderson, A. J.; Bassett, W. A.; Chou, I.-M. *Chem. Phys. Lett.* **2001**, *336*, 212−218.

(4) Barnes, H. L. In *Geochemistry of Hydrothermal Ore Deposits*, Barnes, H. L., Ed.; Wiley: New York, 1979; pp 404−460.

(5) Crerar, D.; Wood, S.; Brantley, S.; Bocarsly, A. *Can. Mineral.* **1985**, *23*, 333−352.

(6) Habenschuss, A.; Spedding, F. H. *J. Phys. Chem.* **1979**, *70*, 2797−2806.

(7) Kurisaki, T.; Yamaguchi, T.; Wakita, H. *J. Alloys Compd.* **1993**, *192*, 293−295.

(8) Helm, L.; Foglia, F.; Kowall, T.; Merbach, A. *J. Phys.* **1994**, *6*, A137−A140.

(9) Cossy, C.; Barnes, A. C.; Enderby, J. E.; Merbach, A. E. *J. Chem. Phys.* **1989**, *90*, 3254−3260.
(10) Wood, S. A.; Tait, C. D.; Janecky, D. R.; Constantopoulos, T. L. *Geochim. Cosmochim. Acta* **1995**, *59*, 5219−5222.
(11) Kanno, H.; Hiraishi, J. J. *Phys. Chem.* **1984**, *88*, 2787−2792.
(12) Yamaguchi, T.; Nomura, M.; Wakita, H.; Ohtaki, H. J. *Chem. Phys.* **1988**, *89*, 5153−5159.
(13) Yaita, T.; Narita, H.; Suzuki, S.; Tachimori, S.; Motohashi, H.; Shiwaku, H. *J. Radioanal. Nucl. Chem.* **1999**, *239*, 371−375.
(14) Allen, P. G.; Butcher, J. J.; Shuh, D. K.; Edelstein, N. M.; Creig, I. *Inorg. Chem.* **2000**, *39*, 595−601.
(15) Ragnarsdottir, K. V.; Oelkers, E. H.; Sherman, D. M.; Collins, C. R. *Chem. Geol*. **1998**, *151*, 29−39.
(16) Haas, J. R.; Shock E. L.; Sassani, D. C. *Geochim. Cosmochim. Acta* **1995**, *59*, 4329−4350.
(17) Wood, S. A. *Chem. Geol.* **1990**, *88*, 99−125.
(18) Wood, S. A.; Wesolowski, D. J.; Palmer, D. A. *Chem. Geol*. **2000**, *167*, 231−253.
(19) Gammons, C. H.; Wood, S. A. *Chem. Geol.* **2000**, *166*, 103−124.
(20) Gammons, C. H.; Wood, S. A.; Williams-Jones, A. E. *Geochim. Cosmochim. Acta* **1996**, *60*, 4615−4630.
(21) Gammons, C. H.; Wood, S. A.; Li, Y. In *Water-Rock Interactions, Ore Deposits, and Environmental Geochemistry: A Tribute to David A. Crear*; Hellmann, R., Wood, S. A., Eds.; The Geochemical Society: St. Louis, MO, 2002; pp 191−207.
(22) Bassett, W. A.; Anderson, A. J.; Mayanovic, R. A.; Chou, I.-M. *Chem. Geol.* **2000**, *167*, 3−10.
(23) Bassett, W. A.; Anderson, A. J.; Mayanovic, R. A.; Chou, I.-M. *Zeit. Kristal.* **2000**, *215*, 711−717.
(24) Anderson, A. J.; Jayanetti, S.; Mayanovic, R. A.; Bassett, W. A.; Chou, I.-M. *Am. Mineral.* **2002**, *87*, 262−268.
(25) Bassett, W. A.; Shen, A. H.; Bucknam, M.; Chou, I.-M. *Rev. Sci. Instr.* **1993**, *64*, 2340−2345.
(26) Jayanetti, S.; Mayanovic, R. A.; Anderson, A. J.; Bassett, W. A.; Chou, I.-M. *J. Chem. Phys.* **2001**, *115*, 954−962.
(27) Newville, M.; Livins, P.; Yacoby, Y.; Rehr, J. J.; Stern, E. A. *Phys. Rev. B* **1993**, *47*, 14126−14131.
(28) Newville, M.; Ravel, B.; Haskel, D.; Rehr, J. J.; Stern, E. A.; Yacoby, Y. *Physica B* **1995**, *208 209*, 154−156.
(29) Stern, E. A.; Newville, M.; Ravel, B.; Yacoby, Y.; Haskel, D. *Physica B* **1995**, *208 209*, 117−120.
(30) Ankudinov, A. L.; Ravel, B.; Rehr, J. J.; Conradson, S. D. *Phys. Rev. B* **1998**, *58*, 7565−7576.
(31) Sayers, D. E.; Bunker, B. A. In *X-ray Absorption: Principles, Applications, Techniques of EXAFS, SEXAFS and XANES*; Koningsberger, D. C., Prins, R., Eds.; Wiley: New York, 1988; pp 211−256.
(32) Recent measurements on Y^{3+} ions in aqueous solution by our group indicate significant diffusion of these ions into the walls of capillaries under varying P−T conditions, including ambient conditions.
(33) Kowall, Th.; Foglia, F.; Helm, L.; Merbach, A. E. *J. Phys. Chem.* **1995**, *99*, 13078−13087.
(34) Fulton, J. L.; Pfund, D. M.; Wallen, S. L.; Newville, M.; Stern, E. A.; Ma, Y. *J. Chem. Phys.* **1996**, *105*, 2161−2166.
(35) Seward, T. M.; Henderson, C. M. B.; Charnock, J. M.; Dobson, B. R. *Geochim. Cosmochim. Acta* **1996**, *60*, 2273−2282.
(36) Seward, T. M.; Henderson, C. M. B.; Charnock, J. M.; Driesner, T. *Geochim. Cosmochim. Acta* **1999**, *63*, 2409−2418.
(37) Pfund, D. M.; Darab, J. G.; Fulton, J. L.; Ma, Y. *J. Phys. Chem.* **1994**, *98*, 13102−13107.
(38) Wallen, S. L.; Palmer, B. J.; Fulton, J. L. *J. Chem. Phys.* **1998**, *108*, 4039−4046.
(39) Hoffman, M. M.; Darab, J. G.; Palmer, B. J.; Fulton, J. L. *J. Phys. Chem.* **1999**, *103*, 8471−8482.
(40) The lack of resolution of individual features in the Fourier transform data attributed to chlorine and oxygen backscatterers, respectively, is due to the finite range of the $\chi(k)$ data and relatively close Yb−Cl and Yb−O distances.
(41) Anderson, A. J.; Mayanovic, R. A.; Bajt, S. *Can. Miner.* **1998**, *36*, 511−524.
(42) Mayanovic, R. A.; Anderson, A. J.; Bassett, W. A.; Chou, I.-M. *J. Synchr. Rad.* **1999**, *6*, 195−197.
(43) Mayanovic, R. A.; Anderson, A. J.; Bajt, S. *Mater. Res. Soc. Proc.* **1997**, *437*, 201−206.
(44) Anderson, A. J.; Mayanovic, R. A.; Bassett, W. A.; Chou, I.-M. In *Steam, Water, and Hydrothermal Systems: Physics and Chemistry Meeting the Needs of Industry*; Tremaine, P. R., et al., Eds.; NRC Research Press: Ottawa, 2000; pp 599−606.
(45) Mayanovic, R. A.; Anderson, A. J.; Bajt, S. *J. Phys. IV France* **1997**, *7*, C2-1029-1030.
(46) Crozier, E. D.; Rehr, J. J.; Ingalls, R. In *X-ray Absorption: Principles, Applications, Techniques of EXAFS, SEXAFS, and XANES*; Koningsberger, D. C., Prins, R., Eds.; Wiley: New York, 1988; pp 373−442.
(47) Weare, J. H. In *Eleventh Annual V. M. Goldschmidt Conference*; Abstract #3871. LPI Contr. No. 1088; Lunar and Planetary Institute: Houston, 2001 (CD-ROM).
(48) Lubin, M. I.; Bylaska, E. J.; Weare, J. H. *Chem. Phys. Lett.* **2000**, *322*, 447−453.
(49) Kowall, Th.; Foglia, F.; Helm, L.; Merbach, A. E. *J. Am. Chem. Soc.* **1995**, *117*, 3790−3799.
(50) Grauch, R. I. In *Geochemistry and Mineralogy or Rare Earth Elements*; Lipin, B. R., McKay, G. A., Eds.; Mineral. Soc. Am.: New York, 1989; pp 147−167.
(51) Giere, R. In *Rare Earth Minerals; Chemistry, origin and ore deposits*; Jones, A. P., Wall, F., Williams, C. T., Eds.; Mineral. Soc. Ser. 7; Chapman & Hall: New York, 1996; pp 105−150.